

Acceleration of ultra-high-energy cosmic rays in the kiloparsec-scale jets of nearby radio galaxies

JIE-SHUANG WANG (王界双) ^{1,2} BRIAN REVILLE ¹ FRANK M. RIEGER ^{2,3,1} AND FELIX A. AHARONIAN ^{4,1,5}

¹*Max-Planck-Institut für Kernphysik, Saupfercheckweg 1, D-69117 Heidelberg, Germany*

²*Max Planck Institute for Plasma Physics, Boltzmannstraße 2, D-85748 Garching, Germany*

³*Institute for Theoretical Physics, Heidelberg University, Philosophenweg 12, D-69120 Heidelberg, Germany*

⁴*Dublin Institute for Advanced Studies, 31 Fitzwilliam Place, Dublin 2, Ireland*

⁵*Yerevan State University, Alek Manukyan St 1, Yerevan 0025, Armenia*

(Received ; Revised ; Accepted)

Submitted to

ABSTRACT

Radio galaxies have long been considered as potential sources of ultra-high-energy cosmic rays (UHECRs). Recent analyses of the UHECR spectrum, composition, and arrival directions indicate that the nearest radio galaxy, Centaurus A, could be linked to the reported dipole anisotropy, though the mechanism underlying the acceleration remains elusive. In this Letter, we explore UHECR acceleration in the kiloparsec-scale jets of radio galaxies, exemplified by Centaurus A. Using high-resolution relativistic magneto-hydrodynamic and test-particle simulations without sub-grid physics, we investigate the acceleration of the highest-energy particles in the turbulent sheath of a fast-moving jet. Our findings demonstrate that acceleration close to the maximum theoretical expectation is possible. When extrapolated to nearby radio galaxies, our results suggest that the kiloparsec-scale jets of Centaurus A could account for the dipole anisotropy in UHECRs, while more potent Fanaroff-Riley type II radio galaxies may account for the observed UHECR spectrum with a rigidity cutoff at a few Exavolts.

1. INTRODUCTION

The origin of ultra-high-energy cosmic rays (UHECRs, $E \gtrsim 1 \text{ EeV} = 10^{18} \text{ eV}$) remains an unsolved problem. Observationally, significant advances have been made recently, thanks to data collected by the Pierre Auger Observatory (PAO) and the Telescope Array experiment. In particular, the extragalactic origin of UHECRs is now corroborated by the detection of a dipole anisotropy in the arrival directions of UHECRs (Pierre Auger Collaboration et al. 2017; Aab et al. 2018). UHECR measurements (Aab et al. 2020a,b; Tsunesada et al. 2021; Abbasi et al. 2023) have revealed several features in the all-particle spectrum, including the *ankle* at $\approx 5 \text{ EeV}$, an *insep* at $\approx 13 \text{ EeV}$, and a cut-off at $\approx 50 \text{ EeV}$, with individual events detected up to $\approx 300 \text{ EeV}$ (Bird et al. 1995; Abbasi et al. 2023). Combined analyses of the spectrum and composition data do favour a scenario in which the UHECR flux has a mixed composition, changing from protons to heavier elements with a hard spectrum and cutoff at a rigidity ($\equiv E/Z_e$) of a few EV (e.g., Aab et al. 2017, 2020b; Abdul Halim et al. 2023), where Z_e is the charge of a given atom. When arrival directions are taken into account, the findings suggest that the nearby active galaxy Centaurus A, hereafter Cen A, could dominate the observed anisotropy signal (Abdul Halim et al. 2024). In addition, the arrival directions of UHECRs $\gtrsim 32 \text{ EeV}$ suggest a hotspot in the direction of Cen A (Abreu et al. 2022; Abdul Halim et al. 2023a).

Jets from Active Galactic Nuclei (AGN) have long been considered as promising UHECR sources (e.g., Hillas 1984; Blandford 2000; Aharonian et al. 2002). Recent studies have shown that the UHECR spectrum and anisotropy could be related to their relativistic jets (e.g., Eichmann et al. 2018; Matthews et al. 2018; Eichmann et al. 2022). However, the mechanisms responsible for accelerating particles to these extreme energies are still uncertain. In the case of the powerful, highly relativistic jets in Fanaroff-Riley (FR) type II radio galaxies, it has been suggested that UHECR

acceleration could occur at their fast jet termination shocks (Rachen & Biermann 1993; Cerutti & Giacinti 2023; Huang et al. 2023), at sub-relativistic shocks in the jets’ back-flows (Matthews et al. 2019; Bell et al. 2019) or at a sharp velocity transition on the jets’ edge (Ostrowski 1998; Rieger & Duffy 2004; Caprioli 2015; Kimura et al. 2018; Mbarek & Caprioli 2021; Seo et al. 2023). In less powerful, mildly-relativistic FR I type sources, UHECR acceleration by stochastic processes has been considered to occur within their large-scale lobes (Hardcastle et al. 2009; O’Sullivan et al. 2009) or in gradual velocity-shearing jet flows (Rieger & Duffy 2004; Rieger et al. 2007; Liu et al. 2017; Webb et al. 2018, 2019; Rieger & Duffy 2019; Lemoine 2019; Webb et al. 2020; Wang et al. 2021; Rieger & Duffy 2022; Wang et al. 2023). Relativistic magneto-hydrodynamic (RMHD) simulations show that Kelvin–Helmholtz driven sheaths form at the interface between the jet spine and the cocoon, indicating that shear acceleration may in fact be a generic mechanism in mildly relativistic jets (Wang et al. 2023).

The UHECR candidate source Cen A is the nearest FR I radio galaxy at a distance of $D \approx 3.8$ Mpc (Harris et al. 2010) and well-studied across the electromagnetic spectrum (e.g. Israel 1998). High-energy observations of its kpc-scale jet favor a synchrotron origin of the X-ray and an inverse Compton origin of the TeV emission (H. E. S. S. Collaboration et al. 2020). These findings imply that efficient (in-situ) acceleration of electrons takes place along the length of its jet. Shear acceleration of particles provides a natural explanation for this (Wang et al. 2021). Interestingly, the observed jet speeds in Cen A are rather mildly relativistic ($\beta \sim 0.5 - 0.7$) (e.g., Hardcastle et al. 2003; Snios et al. 2019), disfavoring acceleration processes that rely on large ($\Gamma > 5$) bulk Lorentz factors. Similar constraints apply to many FR II sources where radio observations indicate rather mildly relativistic bulk velocities for their kpc-scale jets (e.g. Wardle & Aaron 1997; Hardcastle et al. 1999; Arshakian & Longair 2004; Mullin & Hardcastle 2009; Hardcastle & Croston 2020). Modeling of the kpc-scale jet emission in FR II radio galaxies indeed shows that their radio to X-ray spectrum can be reproduced within a framework of electron shear acceleration with a jet bulk velocity $\beta \sim 0.9$ (Wang et al. 2021; He et al. 2023). These findings suggest that efficient shear acceleration of electrons could occur in both FR I and FR II jets, and motivates a related analysis of its role for cosmic-ray energization.

In this Letter, we explore whether UHECRs can be accelerated in the large-scale jets of radio galaxies, taking Cen A as a prime example. We perform dedicated RMHD simulations, tracking test particles using the PLUTO code (Mignone et al. 2007, 2018). Our setup differs from previous studies that explored strongly magnetized flows or highly relativistic jets (e.g., Mbarek & Caprioli 2021; Medina-Torrejón et al. 2023). We explicitly focus on input parameters for the magnetic field and velocity as inferred from earlier analytical modelling of multi-wavelength observations of Cen A, and employ high-resolution simulation to properly probe the growth of instabilities and gyro-motion of the test particles. In Section 2, we introduce our simulation setup. The results are shown in Section 3. The conclusion and implication on understanding the origin of UHECRs are provided in Section 4.

2. SIMULATION SETUP

In order to probe the acceleration process, RMHD simulations are performed, building on previous findings (Wang et al. 2023), but using a significantly increased resolution. The simulation details are provided in Table 1, summarizing the key parameters. The simulations are performed in a three-dimensional Cartesian geometry with the jet’s bulk motion directed along the y -axis. The simulation volume is $2l_0 \times l_0 \times 2l_0$, where length l_0 and grid resolution Δl are defined in Table 1. The cylindrical jet is initialized with a uniform axial velocity β_0 in the spine with radius R_0 , i.e., $\boldsymbol{\beta} = \beta_0 \hat{\mathbf{y}}$ for $r < R_0$ and zero otherwise. Small transverse velocity perturbations are applied at the jet edge (Rossi et al. 2008). Periodic boundary conditions are adopted in the y direction, with outflow boundary conditions used in the x and z .

To mimic the kpc-scale jet of Cen A, we set $\beta_0 = 0.6$ (Hardcastle et al. 2003; Snios et al. 2019) and label these simulations as ‘FR Ia, Ib, Ic’. Radio and X-ray observations (e.g., Hardcastle et al. 2003, 2006; Kraft et al. 2009) suggest that this large-scale jet has a radius of order $R_0 = 0.1$ kpc and a (projected) length of about 4.5 kpc. On smaller scales, the inclination angle of the jet axis wrt the line of sight is constrained to $12^\circ - 45^\circ$ (e.g., Janssen et al. 2021). This suggests a physical (de-projected) jet length $Z_{\text{CenA}} \sim (6 - 22)$ kpc, and a minimum propagation time $t_{\text{jet,min}} \approx Z_{\text{CenA}}/\beta_0 c \sim (110 - 360)R_0/c \sim 10^5$ yrs.

To enable comparison with FR II type jets, we also simulate a jet with $\beta_0 = 0.9$ (e.g. Wardle & Aaron 1997; Hardcastle et al. 1999; Arshakian & Longair 2004; Mullin & Hardcastle 2009; Hardcastle & Croston 2020), labelled ‘FR II’. For this scenario, the initial jet radius is $R_0 = 1$ kpc and is allowed to extend to several hundreds of kpc in length (e.g. Zensus 1997; Wilson et al. 2001; Harris & Krawczynski 2006; Jester et al. 2007; Schwartz et al. 2015;

Blandford et al. 2019; Wang et al. 2021; He et al. 2023), or equivalently a jet propagation time of at least several hundred R_0/c . Particle trajectories are tracked up to $t = 1000R_0/c$.

We simulate jet propagation in a static cocoon. The jet and cocoon are initialized with pressure balance and a temperature $\Theta \equiv p_g/n_0m_p c^2 < 1$ using a Taub-Mathews equation of state (Mathews 1971; Mignone et al. 2005, 2007), where p_g is the gas pressure and m_p is the proton mass. The proper number density of the jet is $n_0 = 10^{-6} \text{ cm}^{-3}$ and the cocoon density is $2n_0$. For the magnetic field we adopt a helical profile with $\langle B_y^2 \rangle = \langle B_\phi^2 \rangle$ for the axial and toroidal components respectively, and define the magnetization parameter $\sigma = \bar{B}_0^2/(8\pi\rho_0 c^2)$, where the average value $\langle f \rangle \equiv \int_0^{R_0} 2\pi f r dr / \int_0^{R_0} 2\pi r dr$ assumes axial symmetry (Wang et al. 2023). The initial mean magnetic field in the spine ($\bar{B}_0 = \sqrt{\langle B_y^2 + B_\phi^2 \rangle}$) and the temperature on the jet axis (Θ_0) are listed in Table 1. Multi-wavelength emission modelling of Cen A suggests a sheath magnetic field strength of $\sim 20\mu\text{G}$ (H. E. S. S. Collaboration et al. 2020; Wang et al. 2021). We take this value for guidance, but allow for some variation in view of the uncertainties in analytic models, and the fact that the observed jet radius of Cen A grows with jet length (Hardcastle et al. 2006). We have studied two magnetizations ($\sigma = 0.02, 0.2$) for our FR Ia-c simulation runs, where the simulated sheaths have nonuniform magnetic fields in the range of $\sim 10 - 60 \mu\text{G}$ (see Figure 2).

In our test-particle simulations, we inject energetic protons as test particles at $t = 0$ to co-evolve with the RMHD simulations. The test particles are injected over the whole jet length within a radial zone Δr_{inj} , with the same injection Lorentz factor (γ_{inj}) as listed in Table 1. In each cell within the injection region, we inject one particle with a random initial direction. The injection energy is chosen such that the particle Larmor radius is few grid cells in length, $\bar{r}_{L,\text{inj}} \sim (2 - 4)\Delta l$, and thus energetic enough to sample the resolved structures formed in the sheath. In the case of Cen A, seed energization could be facilitated by particles being (pre-)accelerated along the jet as indicated by multi-wavelength observations (Hardcastle et al. 2006; Kataoka et al. 2006; H. E. S. S. Collaboration et al. 2020), or by external entrainment of cosmic ray particles (Caprioli 2015; Kimura et al. 2018). In total, we have $N_{\text{inj}} = (0.9 - 4.4) \times 10^7$ test particles in each simulation. Different particle injection zones have been tested within $r_{\text{inj}} \leq 1.05R_0$ for the FR Ia simulation run (see Appendix A). The particle injected within $r_{\text{inj}} \in [0.74, 0.9]R_0$ are accelerated to slightly higher energies, but overall the difference in spectra is small. Thus we consider particles injected at $r_{\text{inj}} \in [0.8, 0.9]R_0$ for other simulation runs.

The RMHD simulation and test-particle simulation are advanced in time simultaneously until a time ($t = t_{\text{frozen}}$), which are listed in Table 1. Afterwards, the RMHD simulation is frozen while the test-particle simulation continues to run in the static magnetic and electric fields. The frozen times are selected to be in the saturated KHI stage, where the turbulent kinetic energy of the jet stays almost constant (Wang et al. 2023). In the framework of Fermi II and shear acceleration, acceleration can occur along the whole jet length. In this manner, the choice of the frozen time reflects the acceleration of particles at various locations along the jet with different velocity and magnetic field profiles.

Runs	β_0	t_{frozen} (R_0/c)	R_0 (kpc)	l_0 (R_0)	Δl (pc)	\bar{B}_0 (μG)	Θ_0	γ_{inj}
FR Ia	0.6	120	0.1	2.6	0.5	27.4	0.05	5×10^7
FR Ib	0.6	60	0.1	2.6	0.5	27.4	0.05	5×10^7
FR Ic	0.6	160	0.1	2.6	0.5	86.9	0.05	9×10^7
FR II	0.9	60	1	3.0	6.0	27.4	0.09	3×10^8

Table 1. Key parameters used in the simulations: initial jet-spine velocity (β_0) and radius (R_0), MHD freeze-time (t_{frozen}), simulation box size (l_0), grid size (Δl), initial mean magnetic field \bar{B}_0 , initial jet temperature parameter Θ_0 , and initial Lorentz factor of injected protons (γ_{inj}).

3. SIMULATION RESULTS

Figure 1 shows an example of the magnetic field structure and velocity profile in a simulation of an FR II type jet. While the behaviour of the jet-sheath dynamics and the developed turbulence have been studied previously (Wang et al. 2023), they are now probed over a substantially wider range. The KHI operates at the interface between the spine and the cocoon, and facilitates formation of a turbulent spine-sheath structure. At the saturated KHI stage, the velocity turbulence spectra are consistent with Kolmogorov scaling over nearly two decades (see Appendix B), while the magnetic turbulence exhibits some flattening towards small wavenumbers. To maximise the dynamic range

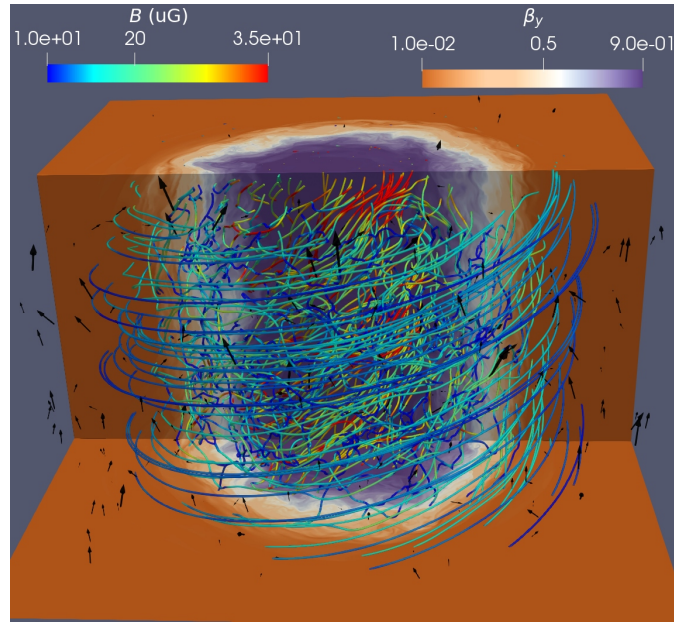


Figure 1. An example of simulation run FR II at $t = t_{\text{frozen}}$. The box size is $6R_0 \times 3R_0 \times 6R_0$. The distribution of the axial velocity β_y is shown in order to illustrate the spine-sheath jet and cocoon structure. Magnetic field lines are shown with color coding of their magnitude. The black arrows represent test particles with larger arrow sizes for higher-energy particles.

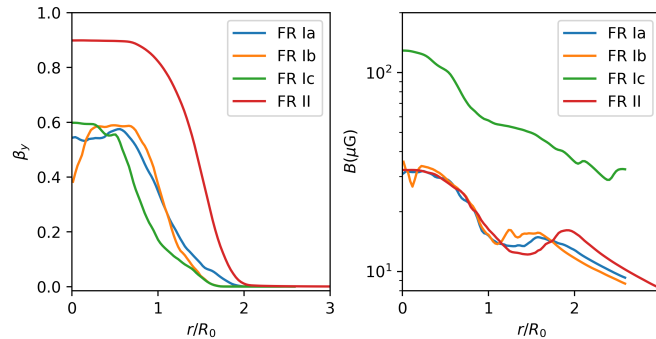


Figure 2. The velocity (left panel) and magnetic field (right panel) profiles in the radial direction are averaged over the axial and azimuthal directions for the simulated jets at the frozen time $t = t_{\text{frozen}}$.

particles are injected at low energies with Larmor radii close to the grid scale. While numerical diffusion results in deviation from Kolmogorov-scaling at the grid-scale, as shown in Figure B2, the results are found to be consistent when injecting at higher energies, as discussed in Appendix C. Therefore, we fix the injection energy for other simulations as shown in Table 1. Averaging over the axial and azimuthal directions, we show examples of the velocity and magnetic field profiles along the radial direction of the spine-sheath jet at $t = t_{\text{frozen}}$ of the simulation runs in Figure 2. Since the jet radius changes over time, we hereinafter re-define the spine-sheath jet radius as the region with $\beta_y \geq 0.01$, i.e., $R_j = r(\langle \beta_y \rangle = 10^{-2})$. In the sheath, the velocity drops smoothly, while the magnetic field displays a pile-up at the edge of the jet in the low-magnetization simulation runs.

In such a shearing turbulent jet sheath, particles are expected to undergo stochastic Fermi II acceleration as well as (gradual) shear acceleration. The latter can also be viewed as a stochastic Fermi-type acceleration process, where charged particles gain energy by scattering off the turbulence embedded in a large-scale sheared flow profile (e.g., Rieger 2019; Lemoine 2019). Figure 3 provides an illustration of these effects. As particles repeatedly traverse the turbulent jet-sheath, they gain energy. To study the potential for UHECR acceleration in such scenarios, we focus on the spectrum and the maximum energy of the simulated particles below. For the analysis of the particle spectra, we take only particles inside the jet (at $r \leq R_j$) into account.

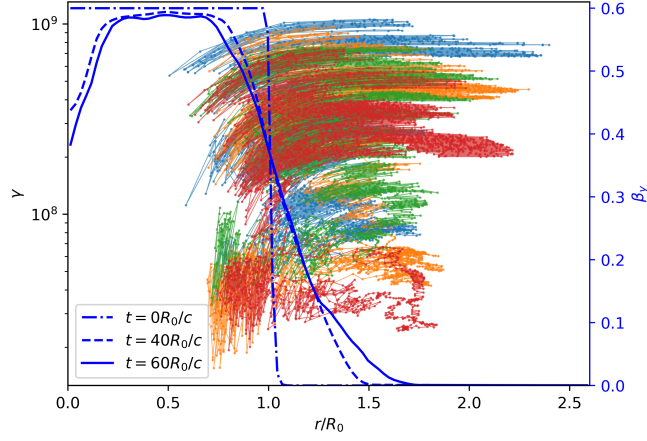


Figure 3. Exemplary trajectories of four test particles are shown with different colors for the FR Ib simulation run. The trajectories are projected in the radial direction of the jet. The left y -axis is the Lorentz factor (γ) of test particles. The blue lines are the velocity profiles of the jet at different simulation times, with the values shown at the right y -axis.

In Figure 4 we show the time evolution of the particle spectra for the FR I and FR II simulation runs. For the low-magnetization FR I jets, we employ two simulation runs at a different MHD frozen time: $t_{\text{frozen}} = 60R_0/c$ (FR Ib) and $t_{\text{frozen}} = 120R_0/c$ (FR Ia). Although protons are injected mono-energetically in the simulation frame, the particle distributions broaden over time, spanning an energy range more than a factor of 10 above the injection energy. This is typical for stochastic acceleration processes. From the FR Ia/b simulation runs, we found that the particle spectra do not change significantly with different choices of frozen time. Thus we perform only one simulation for an FR I jet with a higher magnetization (FR Ic), and one simulation for FR II jets. For both, the FR I and FR II cases, the spectral peak energy and the maximum particle energy increase systematically due to acceleration, with roughly the same spectral shape at $t \geq 120R_0/c$. These results demonstrate that efficient particle acceleration by stochastic processes is operative in mildly relativistic jets with speeds $\beta \sim 0.6 - 0.9$.

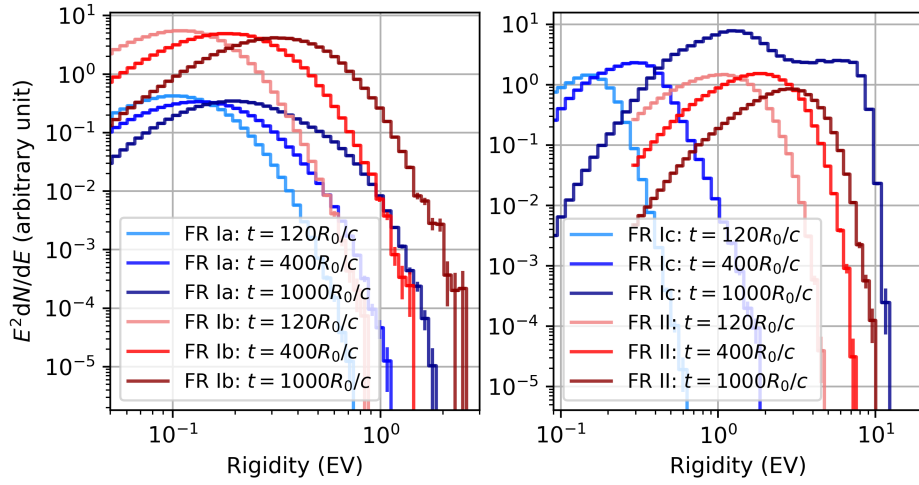


Figure 4. The normalized particle spectra of test particles as obtained at different simulation times $t = 120R_0/c$, $t = 400R_0/c$ and $t = 1000R_0/c$ for the simulation runs FR Ia, Ib (left panel), Ic and FR II (right panel). The normalization factors are chosen differently for the purpose of visualization. To avoid overlapping lines, we only show the particle spectrum above the injection energy.

For the FR Ic simulation, an additional high-energy (HE) component becomes apparent at later time, as shown in Figure 4. To explore the difference between the highest-energy particles and all the particles for the FR I simulations, we investigate the time evolution of the acceleration rate and acceleration location. We select particles with energy $\gamma > 0.5\gamma_{\text{max}}$ for the respective HE component, where γ_{max} is the highest-energy particle in each simulation. We

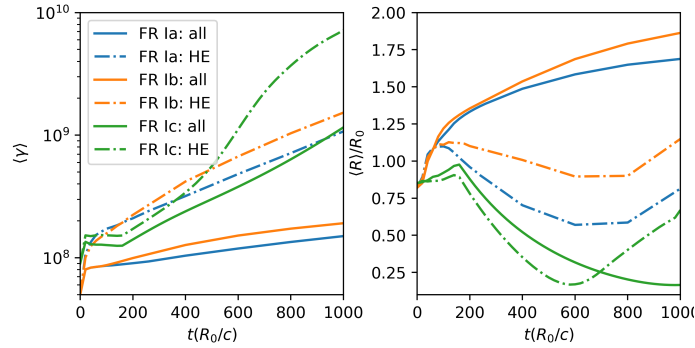


Figure 5. The time evolution of mean energy (left panel) and mean radial position (right panel) for the FR I simulations. The right panel has the same figure legend as the left panel. The solid lines, labeled with ‘all’ are for the all-particle sample. The dashed-dotted lines, labeled with ‘HE’ are for the high-energy component.

subsequently obtain the time evolution of the mean energy ($\langle \gamma \rangle$) and mean radial position ($\langle R \rangle$) for both, the all-particle sample and the HE sample. The results are shown in Figure 5. As can be seen, the evolutionary trends for the FR Ia/b simulations are quite similar, while the FR Ic simulation behaves differently. At later time $t \gtrsim 400R_0/c$, the HE component of the FR Ic simulation reveals an increased acceleration compared to the other simulations. We attribute this visual difference to the higher magnetization employed in our FR Ic simulation that contributes to a separation of stochastic (Fermi II) and shear particle acceleration processes. The mean radial positions show that the all-particle samples systematically moves to the outer/inner edge of the sheath, where in FR Ia/b simulations the trend is to move outwards with $\langle R \rangle / R_0 \gtrsim 1.7 - 1.9$ and to move inwards with $\langle R \rangle / R_0 \lesssim 0.2$ in the FR Ic simulation. However, in general the HE components in these simulations tend to stay in the sheath, experiencing both stochastic and shear acceleration. The HE component of the FR Ic simulation reveals increased acceleration compared to the all-particle sample, primarily occurring when those HE particles move from the spine to the inner sheath, while the all-particle sample continues moving inward. The higher velocity (gradient) and/or the higher magnetic field in the inner sheath may thus contribute to the observed difference in energization. We plan to investigate this in more detail with further simulations in a future paper.

As particles are injected impulsively at $t = 0$ in our simulations, we integrate the spectrum over time to mimic continuous injection. To quantify the acceleration capability, we define a Hillas limit (Hillas 1984) for particles in our simulated jets, $E_{\max} = q\beta R_j$, where R_j is the jet radius at the frozen time $t = t_{\text{frozen}}$. The integrated particle spectra for all simulation runs are shown in Figure 6 along with dotted lines for E_{\max} . It is seen that for different jet magnetizations and velocities, the particle energy spectra peak at around $0.1E_{\max}$. Below the peak, the time-integrated spectra are as hard as $dN/dE \propto E^{-1}$, which are compatible with efficient stochastic-shear acceleration and ineffective escape. A more complex situation concerning particle escape could arise in the case of significant pre-existing magnetic turbulence in the cocoon. In the case of shear acceleration, the acceleration efficiency depends on the velocity profile of the jet with a sharper velocity-shearing flow (larger flow gradients), leading to more efficient acceleration (e.g., Webb et al. 2018; Rieger & Duffy 2019). As shown in Figure 2 the FR Ib simulation run exhibits a steeper velocity gradient in the sheath, which could account for the difference in the spectra compared to that of the FR Ia simulation run. For the FR Ic simulation, individual particles do reach beyond the noted Hillas limit. Note, however, if we take the jet diameter instead of the radius as the system size, those particles would be within the limit.

4. CONCLUSIONS

In this letter, we have explored the possibility for a source such as Cen A to accelerate particles to multi-EeV energies via stochastic Fermi-type processes. Cen A is particularly interesting as the UHECR candidate source that could provide the dominant contribution to the observed anisotropy signal (e.g., Abdul Halim et al. 2024). Based on observations of its current large-scale jet, the available time for the acceleration of particles is at least $t_{\text{jet, min}} \sim (110 - 360)R_0/c$ as estimated above. For a jet speed of $\beta_0 = 0.6$ and a magnetization of $\sigma = 0.02 - 0.2$ (FR I simulations), our simulations show that the resultant proton energy spectra ($E^2 dN/dE$) peak at $\sim 0.2 - 0.7$ EeV, and extend beyond 1 EeV. The spectral peak approximately satisfy $E_{\text{peak}} \approx 0.1E_{\max}$ for simulations with different magnetization and velocity parameters. As suggested in the literature (e.g., Matthews et al. 2018), Cen A may have exhibited enhanced activity in the past accounting for its giant radio lobe structure. Our results indicate that in the

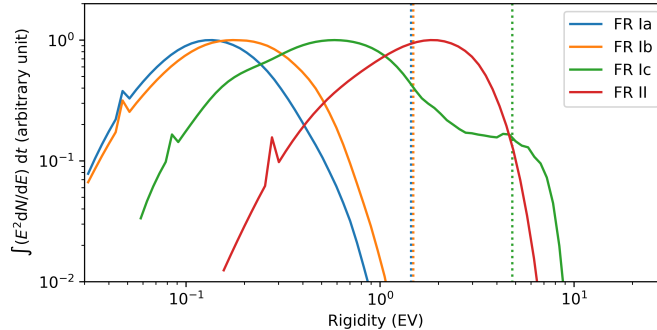


Figure 6. The spectra are integrated over time to mimic continuous particle injections for our simulation runs. The vertical lines denotes the Hillas reference limit for the jet. The spectra are normalized such that the first data points are equal to unity. The spikes in the spectra are an artefact of the mono-energetic injection (see γ_{inj} in Table 1).

presence of larger jet velocities and/or higher jet magnetizations, possibly associated with such a phase, the peak in the proton energy distribution could be shifted to higher energies. Further studies on the multiwavelength jet properties of Cen A will be important to quantify this in more detail.

Analysis of the PAO observations shows that the amplitude of the UHECR dipole anisotropy increases from 1.7% in 4 – 8 EeV to 17% at ≥ 32 EeV (Pierre Auger Collaboration et al. 2017; Aab et al. 2018; Abdul Halim et al. 2023a). The mass composition at those energies is likely a mix of H, He, and CNO-type elements (Abdul Halim et al. 2023b; Coleman et al. 2023). To account for this by Cen A, FR Ic type simulations are favored, where the rigidity spectrum extends well beyond several EV. Heavy elements could in principle enter the jet through mass entrainment by, e.g., stellar material inside the jet (Wykes et al. 2015; Bosch-Ramon 2023), or from the medium surrounding the jet shearing layer (Perucho 2019). Additionally, lower-energy cosmic rays produced within the host galaxy may be picked up by the jet, contributing to variations in the mass composition (Caprioli 2015; Kimura et al. 2018). It seems likely, however, that to properly account for the inferred super-solar UHECR abundance, some further enhancement of heavy elements at the injection scale is needed. To which extent this might be facilitated by an additional pre-acceleration mechanism remains to be investigated. While the accelerated particles in our simulations have a hard spectrum, UHECRs escaping from the jet-cocoon system could reveal an even harder spectrum. This seems in general consistent with the suggested hard UHECR spectrum (e.g., Aab et al. 2017; Ehlert et al. 2023).

While offering important insights, the amplitude of the UHECR anisotropy is $\lesssim 10\%$, indicating that there is a dominant isotropic component. The recent combined analysis of the UHECR spectrum and composition data favours a rigidity cutoff at a few EV (Aab et al. 2017, 2020b; Abdul Halim et al. 2023). It has been suggested that the isotropic UHECR component could originate from more powerful FR II type radio galaxies (e.g., Eichmann et al. 2018; Matthews et al. 2018; Eichmann et al. 2022). Our results provide an illustration that for mildly relativistic FR II type conditions, (rigidity-spectrum) peak energies around ~ 2 EV for $t = (120 - 400)R_0/c$ can be reached. It seems thus likely that UHECRs at 100 EV could represent heavy elements from powerful FR II jets exhibiting higher magnetization and/or larger jet radii.

1 We are grateful to the referee for suggestions. J.S.W. thanks T. Bell and M. Lemoine for discussions. J.S.W. acknowl-
 2 edges support by the Alexander von Humboldt Foundation and F.M.R. by the German Science Foundation (DFG RI
 3 1187/8-1).

Software: PLUTO (Mignone et al. 2007, 2018); NumPy (Harris et al. 2020); Matplotlib (Hunter 2007), ParaView (Ahrens et al. 2005)

Facility: The HPC system Raven from the Max Planck Computing and Data Facility (MPCDF)

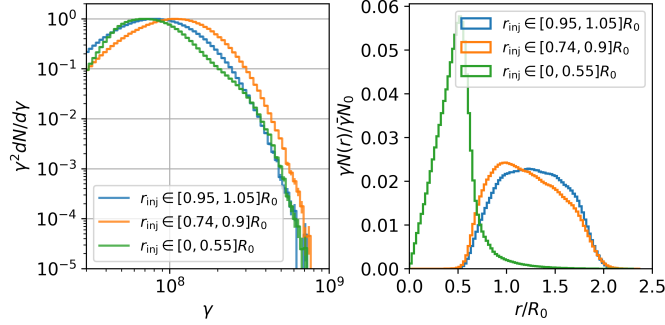


Figure A1. The spectral energy distributions (left panel) and spatial distributions (right panel) are shown for particle injected at different radius at the frozen time $t_{\text{frozen}} = 120R_0/c$. The particle energy spectra are normalized to unity at the peak value, while the spatial distribution are normalized so that the sum of distribution equals to unity.

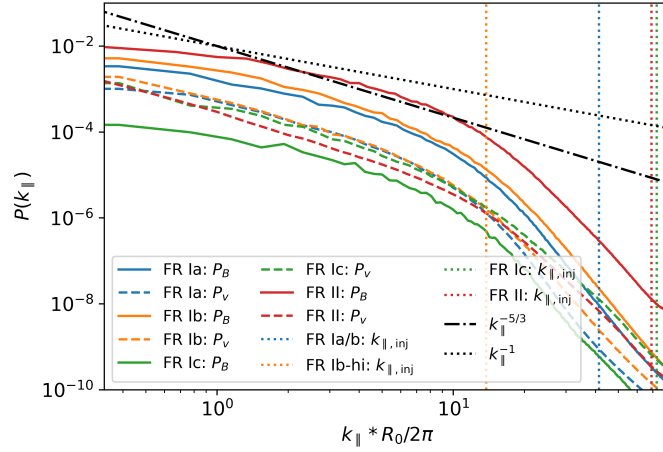


Figure B2. The turbulence spectra for the velocity (P_v) and magnetic field (P_B) are shown for the different simulation runs. The vertical dotted lines corresponds to the average Larmor radii of the injected energy for different simulations (see Sections 3 and Appendix C for details).

A. THE EFFECT OF INJECTION RADIUS

For the FR Ia simulation run, we have injected particles in the region $r_{\text{inj}} \in [0, 0.55]R_0$, $[0.74, 0.9]R_0$, $[0.95, 1.05]R_0$. The test particles co-evolve with the RMHD simulation to the frozen time. At the frozen time, the particle spectral and the spatial distribution are shown in Figure A1. It can be seen that particles spread out spatially to a wide radius range, especially for those particles injected close to the jet boundary, while the difference in the energy spectra is overall small. Particles injected at $r_{\text{inj}} \in [0.74, 0.9]R_0$ have a peak in the inner sheath $r \sim R_0$, and are accelerated to slightly higher energies compared to the other two cases. This is in general consistent with stochastic-shear acceleration, as the inner sheath has a slightly larger velocity gradient.

B. TURBULENCE SPECTRA

Following Wang et al. (2023), we perform a fast Fourier transform of the velocity and magnetic fields along the jet axis with wavenumber k_{\parallel} at the saturated KHI stage ($t = t_{\text{frozen}}$). The minimum and maximum wavenumber are determined by the simulation box-size and grid size, respectively. The results are shown in Figure B2. It can be seen that the power-law component of the power spectra generally extends over approximately two decades within wavenumbers $k_{\parallel}R_0/2\pi \lesssim 10 - 20$. The turbulent velocity spectra are compatible with a Kolmogorov-type turbulence, while the magnetic turbulence reveals some flattening towards small wavenumber, approaching a Bohm scaling (k_{\parallel}^{-1}).

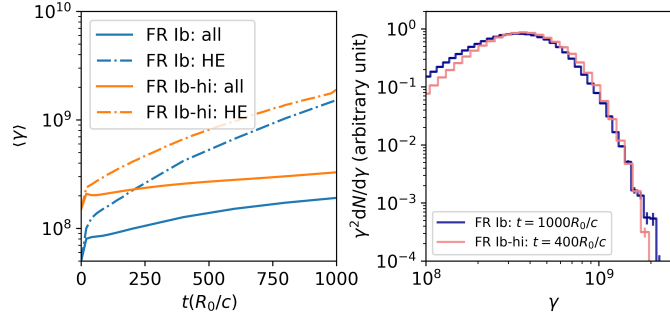


Figure C3. The time evolution of the mean particle energy (left panel) and the spectra (right panel) of the FR Ib and FR Ib-hi simulations. The definition of the all-particle sample and HE component in the left panel are the same as in Figure 5. In the right hand panel, the normalization and particle energy range are selected for visualization purposes, similar to Figure 4.

C. THE EFFECT OF INJECTION ENERGY

As shown in Figure B2, the Larmor radii of the injected particles in the simulations resonate with wavenumbers $k_{\parallel, \text{inj}} R_0 / 2\pi \approx 40 - 70$, which lies beyond Kolmogorov-scaling range. This is unavoidable if we inject close to the grid scale. To determine if this changes any of our conclusions, we thus conducted an additional simulation, FR Ib-hi, based on the initial setup of the FR Ib simulation, only with a higher injection Lorentz factor $\gamma_{\text{inj}} = 1.5 \times 10^8$, corresponding to an average resonant wavenumber $k_{\parallel, \text{inj}} R_0 / 2\pi \approx 14$. We present the time evolution of the mean particle energy and spectra in Figure C3. The mean particle energy in FR Ib simulation reaches $\langle \gamma \rangle \approx 1.5 \times 10^8$ at $t \approx 600 R_0 / c$. Therefore, we compare the results between FR Ib simulation at $t \gtrsim 600 R_0 / c$ and FR Ib-hi simulation at $t \lesssim 400 R_0 / c$. Our results show that the mean acceleration rates ($d \log \langle \gamma \rangle / dt$) for both the all-particle sample and HE component and the spectra for FR Ib simulation at $t = 1000 R_0 / c$ and FR Ib-hi simulation at $t = 400 R_0 / c$ are comparable. This indicates that variations in injection energy do not significantly affect the results. The reason could be that the particle spectra in the FR Ib simulation peak above a Lorentz factor of 1.5×10^8 at $t \gtrsim 120 R_0 / c$ (Figure 4), and the average particle energy reaches this scale in a time $t \gtrsim 600 R_0 / c$. These particles can experience the Kolmogorov-type turbulence with $k_{\parallel} R_0 / 2\pi \lesssim 14$ for a long duration of time, such that the result resembles that of the FR Ib-hi simulation with an injection energy $\gamma_{\text{inj}} = 1.5 \times 10^8$.

REFERENCES

- Aab, A., Abreu, P., Aglietta, M., et al. 2017, JCAP, 2017, 038, doi: [10.1088/1475-7516/2017/04/038](https://doi.org/10.1088/1475-7516/2017/04/038)
- . 2018, ApJ, 868, 4, doi: [10.3847/1538-4357/aae689](https://doi.org/10.3847/1538-4357/aae689)
- . 2020a, PhRvD, 102, 062005, doi: [10.1103/PhysRevD.102.062005](https://doi.org/10.1103/PhysRevD.102.062005)
- . 2020b, PhRvL, 125, 121106, doi: [10.1103/PhysRevLett.125.121106](https://doi.org/10.1103/PhysRevLett.125.121106)
- Abbasi, R. U., Abe, Y., Abu-Zayyad, T., et al. 2023, Astroparticle Physics, 151, 102864, doi: [10.1016/j.astropartphys.2023.102864](https://doi.org/10.1016/j.astropartphys.2023.102864)
- Abbasi, R. U., Allen, M. G., Arimura, R., et al. 2023, Science, 382, 903, doi: [10.1126/science.abo5095](https://doi.org/10.1126/science.abo5095)
- Abdul Halim, A., Abreu, P., Aglietta, M., et al. 2023, JCAP, 2023, 024, doi: [10.1088/1475-7516/2023/05/024](https://doi.org/10.1088/1475-7516/2023/05/024)
- Abdul Halim, A., Abreu, P., Aglietta, M., et al. 2023a, in Proceedings of 38th International Cosmic Ray Conference — PoS(ICRC2023), Vol. 444, 252, doi: [10.22323/1.444.0252](https://doi.org/10.22323/1.444.0252)
- Abdul Halim, A., Abreu, P., Aglietta, M., et al. 2023b, in Proceedings of 38th International Cosmic Ray Conference — PoS(ICRC2023), Vol. 444, 438, doi: [10.22323/1.444.0438](https://doi.org/10.22323/1.444.0438)
- . 2024, JCAP, 2024, 022, doi: [10.1088/1475-7516/2024/01/022](https://doi.org/10.1088/1475-7516/2024/01/022)
- Abreu, P., Aglietta, M., Albury, J. M., et al. 2022, ApJ, 935, 170, doi: [10.3847/1538-4357/ac7d4e](https://doi.org/10.3847/1538-4357/ac7d4e)
- Aharonian, F. A., Belyanin, A. A., Derishev, E. V., Kocharovskiy, V. V., & Kocharovskiy, V. V. 2002, PhRvD, 66, 023005, doi: [10.1103/PhysRevD.66.023005](https://doi.org/10.1103/PhysRevD.66.023005)
- Ahrens, J., Geveci, B., & Law, C. 2005, in Visualization Handbook (Elsevier)
- Arshakian, T. G., & Longair, M. S. 2004, MNRAS, 351, 727, doi: [10.1111/j.1365-2966.2004.07823.x](https://doi.org/10.1111/j.1365-2966.2004.07823.x)
- Bell, A. R., Matthews, J. H., Blundell, K. M., & Araudo, A. T. 2019, MNRAS, 487, 4571, doi: [10.1093/mnras/stz1604](https://doi.org/10.1093/mnras/stz1604)

- Bird, D. J., Corbato, S. C., Dai, H. Y., et al. 1995, *ApJ*, 441, 144, doi: [10.1086/175344](https://doi.org/10.1086/175344)
- Blandford, R., Meier, D., & Readhead, A. 2019, *ARA&A*, 57, 467, doi: [10.1146/annurev-astro-081817-051948](https://doi.org/10.1146/annurev-astro-081817-051948)
- Blandford, R. D. 2000, *PhST*, 85, 191, doi: [10.1238/Physica.Topical.085a00191](https://doi.org/10.1238/Physica.Topical.085a00191)
- Bosch-Ramon, V. 2023, *A&A*, 677, L14, doi: [10.1051/0004-6361/202347554](https://doi.org/10.1051/0004-6361/202347554)
- Caprioli, D. 2015, *ApJL*, 811, L38, doi: [10.1088/2041-8205/811/2/L38](https://doi.org/10.1088/2041-8205/811/2/L38)
- Cerutti, B., & Giacinti, G. 2023, *A&A*, 676, A23, doi: [10.1051/0004-6361/202346481](https://doi.org/10.1051/0004-6361/202346481)
- Coleman, A., Eser, J., Mayotte, E., et al. 2023, *APh*, 147, 102794, doi: [10.1016/j.astropartphys.2022.102794](https://doi.org/10.1016/j.astropartphys.2022.102794)
- Ehlert, D., Oikonomou, F., & Unger, M. 2023, *PhRvD*, 107, 103045, doi: [10.1103/PhysRevD.107.103045](https://doi.org/10.1103/PhysRevD.107.103045)
- Eichmann, B., Kachelrieß, M., & Oikonomou, F. 2022, *JCAP*, 2022, 006, doi: [10.1088/1475-7516/2022/07/006](https://doi.org/10.1088/1475-7516/2022/07/006)
- Eichmann, B., Rachen, J. P., Merten, L., van Vliet, A., & Becker Tjus, J. 2018, *JCAP*, 2018, 036, doi: [10.1088/1475-7516/2018/02/036](https://doi.org/10.1088/1475-7516/2018/02/036)
- H. E. S. S. Collaboration, Abdalla, H., Adam, R., et al. 2020, *Nature*, 582, 356, doi: [10.1038/s41586-020-2354-1](https://doi.org/10.1038/s41586-020-2354-1)
- Hardcastle, M. J., Alexander, P., Pooley, G. G., & Riley, J. M. 1999, *MNRAS*, 304, 135, doi: [10.1046/j.1365-8711.1999.02298.x](https://doi.org/10.1046/j.1365-8711.1999.02298.x)
- Hardcastle, M. J., Cheung, C. C., Feain, I. J., & Stawarz, L. 2009, *MNRAS*, 393, 1041, doi: [10.1111/j.1365-2966.2008.14265.x](https://doi.org/10.1111/j.1365-2966.2008.14265.x)
- Hardcastle, M. J., & Croston, J. H. 2020, *NewAR*, 88, 101539, doi: [10.1016/j.newar.2020.101539](https://doi.org/10.1016/j.newar.2020.101539)
- Hardcastle, M. J., Kraft, R. P., & Worrall, D. M. 2006, *MNRAS*, 368, L15, doi: [10.1111/j.1745-3933.2006.00146.x](https://doi.org/10.1111/j.1745-3933.2006.00146.x)
- Hardcastle, M. J., Worrall, D. M., Kraft, R. P., et al. 2003, *ApJ*, 593, 169, doi: [10.1086/376519](https://doi.org/10.1086/376519)
- Harris, C. R., Millman, K. J., van der Walt, S. J., et al. 2020, *Nature*, 585, 357, doi: [10.1038/s41586-020-2649-2](https://doi.org/10.1038/s41586-020-2649-2)
- Harris, D. E., & Krawczynski, H. 2006, *ARA&A*, 44, 463, doi: [10.1146/annurev.astro.44.051905.092446](https://doi.org/10.1146/annurev.astro.44.051905.092446)
- Harris, G. L. H., Rejkuba, M., & Harris, W. E. 2010, *PASA*, 27, 457, doi: [10.1071/AS09061](https://doi.org/10.1071/AS09061)
- He, J.-C., Sun, X.-N., Wang, J.-S., et al. 2023, *MNRAS*, 525, 5298, doi: [10.1093/mnras/stad2542](https://doi.org/10.1093/mnras/stad2542)
- Hillas, A. M. 1984, *ARA&A*, 22, 425, doi: [10.1146/annurev.aa.22.090184.002233](https://doi.org/10.1146/annurev.aa.22.090184.002233)
- Huang, Z.-Q., Reville, B., Kirk, J. G., & Giacinti, G. 2023, *MNRAS*, 522, 4955, doi: [10.1093/mnras/stad1356](https://doi.org/10.1093/mnras/stad1356)
- Hunter, J. D. 2007, *Computing in Science & Engineering*, 9, 90, doi: [10.1109/MCSE.2007.55](https://doi.org/10.1109/MCSE.2007.55)
- Israel, F. P. 1998, *A&AR*, 8, 237, doi: [10.1007/s001590050011](https://doi.org/10.1007/s001590050011)
- Janssen, M., Falcke, H., Kadler, M., et al. 2021, *Nature Astronomy*, 5, 1017, doi: [10.1038/s41550-021-01417-w](https://doi.org/10.1038/s41550-021-01417-w)
- Jester, S., Meisenheimer, K., Martel, A. R., Perlman, E. S., & Sparks, W. B. 2007, *MNRAS*, 380, 828, doi: [10.1111/j.1365-2966.2007.12120.x](https://doi.org/10.1111/j.1365-2966.2007.12120.x)
- Kataoka, J., Stawarz, L., Aharonian, F., et al. 2006, *ApJ*, 641, 158, doi: [10.1086/500407](https://doi.org/10.1086/500407)
- Kimura, S. S., Murase, K., & Zhang, B. T. 2018, *PhRvD*, 97, 023026, doi: [10.1103/PhysRevD.97.023026](https://doi.org/10.1103/PhysRevD.97.023026)
- Kraft, R. P., Forman, W. R., Hardcastle, M. J., et al. 2009, *ApJ*, 698, 2036, doi: [10.1088/0004-637X/698/2/2036](https://doi.org/10.1088/0004-637X/698/2/2036)
- Lemoine, M. 2019, *PhRvD*, 99, 083006, doi: [10.1103/PhysRevD.99.083006](https://doi.org/10.1103/PhysRevD.99.083006)
- Liu, R.-Y., Rieger, F. M., & Aharonian, F. A. 2017, *ApJ*, 842, 39, doi: [10.3847/1538-4357/aa7410](https://doi.org/10.3847/1538-4357/aa7410)
- Mathews, W. G. 1971, *ApJ*, 165, 147, doi: [10.1086/150883](https://doi.org/10.1086/150883)
- Matthews, J. H., Bell, A. R., Blundell, K. M., & Araudo, A. T. 2018, *MNRAS*, 479, L76, doi: [10.1093/mnrasl/sly099](https://doi.org/10.1093/mnrasl/sly099)
- . 2019, *MNRAS*, 482, 4303, doi: [10.1093/mnras/sty2936](https://doi.org/10.1093/mnras/sty2936)
- Mbarek, R., & Caprioli, D. 2021, *ApJ*, 921, 85, doi: [10.3847/1538-4357/ac1da8](https://doi.org/10.3847/1538-4357/ac1da8)
- Medina-Torrejón, T. E., de Gouveia Dal Pino, E. M., & Kowal, G. 2023, *ApJ*, 952, 168, doi: [10.3847/1538-4357/acd699](https://doi.org/10.3847/1538-4357/acd699)
- Mignone, A., Bodo, G., Massaglia, S., et al. 2007, *ApJS*, 170, 228, doi: [10.1086/513316](https://doi.org/10.1086/513316)
- Mignone, A., Bodo, G., Vaidya, B., & Mattia, G. 2018, *ApJ*, 859, 13, doi: [10.3847/1538-4357/aabccd](https://doi.org/10.3847/1538-4357/aabccd)
- Mignone, A., Plewa, T., & Bodo, G. 2005, *ApJS*, 160, 199, doi: [10.1086/430905](https://doi.org/10.1086/430905)
- Mullin, L. M., & Hardcastle, M. J. 2009, *MNRAS*, 398, 1989, doi: [10.1111/j.1365-2966.2009.15232.x](https://doi.org/10.1111/j.1365-2966.2009.15232.x)
- Ostrowski, M. 1998, *A&A*, 335, 134, doi: [10.48550/arXiv.astro-ph/9803299](https://doi.org/10.48550/arXiv.astro-ph/9803299)
- O'Sullivan, S., Reville, B., & Taylor, A. M. 2009, *MNRAS*, 400, 248, doi: [10.1111/j.1365-2966.2009.15442.x](https://doi.org/10.1111/j.1365-2966.2009.15442.x)
- Perucho, M. 2019, *Galax*, 7, 70, doi: [10.3390/galaxies7030070](https://doi.org/10.3390/galaxies7030070)
- Pierre Auger Collaboration, Aab, A., Abreu, P., et al. 2017, *Science*, 357, 1266, doi: [10.1126/science.aan4338](https://doi.org/10.1126/science.aan4338)
- Rachen, J. P., & Biermann, P. L. 1993, *A&A*, 272, 161, doi: [10.48550/arXiv.astro-ph/9301010](https://doi.org/10.48550/arXiv.astro-ph/9301010)
- Rieger, F. M. 2019, *Galaxies*, 7, 78, doi: [10.3390/galaxies7030078](https://doi.org/10.3390/galaxies7030078)
- Rieger, F. M., Bosch-Ramon, V., & Duffy, P. 2007, *Ap&SS*, 309, 119, doi: [10.1007/s10509-007-9466-z](https://doi.org/10.1007/s10509-007-9466-z)

- Rieger, F. M., & Duffy, P. 2004, *ApJ*, 617, 155,
doi: [10.1086/425167](https://doi.org/10.1086/425167)
- . 2019, *ApJL*, 886, L26, doi: [10.3847/2041-8213/ab563f](https://doi.org/10.3847/2041-8213/ab563f)
- . 2022, *ApJ*, 933, 149, doi: [10.3847/1538-4357/ac729c](https://doi.org/10.3847/1538-4357/ac729c)
- Rossi, P., Mignone, A., Bodo, G., Massaglia, S., & Ferrari, A. 2008, *A&A*, 488, 795,
doi: [10.1051/0004-6361:200809687](https://doi.org/10.1051/0004-6361:200809687)
- Schwartz, D. A., Marshall, H. L., Worrall, D. M., et al. 2015, in *Extragalactic Jets from Every Angle*, ed. F. Massaro, C. C. Cheung, E. Lopez, & A. Siemiginowska, Vol. 313, 219–224,
doi: [10.1017/S1743921315002215](https://doi.org/10.1017/S1743921315002215)
- Seo, J., Ryu, D., & Kang, H. 2023, *ApJ*, 944, 199,
doi: [10.3847/1538-4357/acb3ba](https://doi.org/10.3847/1538-4357/acb3ba)
- Snios, B., Wykes, S., Nulsen, P. E. J., et al. 2019, *ApJ*, 871, 248, doi: [10.3847/1538-4357/aafaf3](https://doi.org/10.3847/1538-4357/aafaf3)
- Tsunesada, Y., Abbasi, R., Abu-Zayyad, T., et al. 2021, in *Proceedings of 37th International Cosmic Ray Conference — PoS(ICRC2021)*, Vol. 395, 337,
doi: [10.22323/1.395.0337](https://doi.org/10.22323/1.395.0337)
- Wang, J.-S., Reville, B., Liu, R.-Y., Rieger, F. M., & Aharonian, F. A. 2021, *MNRAS*, 505, 1334,
doi: [10.1093/mnras/stab1458](https://doi.org/10.1093/mnras/stab1458)
- Wang, J.-S., Reville, B., Mizuno, Y., Rieger, F. M., & Aharonian, F. A. 2023, *MNRAS*, 519, 1872,
doi: [10.1093/mnras/stac3616](https://doi.org/10.1093/mnras/stac3616)
- Wardle, J. F. C., & Aaron, S. E. 1997, *MNRAS*, 286, 425,
doi: [10.1093/mnras/286.2.425](https://doi.org/10.1093/mnras/286.2.425)
- Webb, G. M., Al-Nussirat, S., Mostafavi, P., et al. 2019, *ApJ*, 881, 123, doi: [10.3847/1538-4357/ab2fca](https://doi.org/10.3847/1538-4357/ab2fca)
- Webb, G. M., Barghouty, A. F., Hu, Q., & le Roux, J. A. 2018, *ApJ*, 855, 31, doi: [10.3847/1538-4357/aaae6c](https://doi.org/10.3847/1538-4357/aaae6c)
- Webb, G. M., Mostafavi, P., Al-Nussirat, S., et al. 2020, *ApJ*, 894, 95, doi: [10.3847/1538-4357/ab8635](https://doi.org/10.3847/1538-4357/ab8635)
- Wilson, A. S., Young, A. J., & Shopbell, P. L. 2001, *ApJ*, 547, 740, doi: [10.1086/318412](https://doi.org/10.1086/318412)
- Wykes, S., Hardcastle, M. J., Karakas, A. I., & Vink, J. S. 2015, *MNRAS*, 447, 1001, doi: [10.1093/mnras/stu2440](https://doi.org/10.1093/mnras/stu2440)
- Zensus, J. A. 1997, *ARA&A*, 35, 607,
doi: [10.1146/annurev.astro.35.1.607](https://doi.org/10.1146/annurev.astro.35.1.607)